Supplementary Information (SI) for Journal of Materials Chemistry C.
This journal is © The Royal Society of Chemistry 2024

Stronger Polar Ferromagnetism and Narrower Optical Band Gaps in Two-Dimensional Hybrid Copper Perovskites Induced by Bromine-Substitution

Ceng Han,*[,†] Jason A. McNulty,[†] Alasdair J. Bradford,[†,‡] Alexandra M. Z. Slawin,[†] Stephen L. Lee,[‡] and Philip Lightfoot*[,†]

[†]School of Chemistry and EaStChem, University of St Andrews, St Andrews, KY16 9ST, United Kingdom

[‡]School of Physics, University of St Andrews, St Andrews, Fife, KY16 9SS, United Kingdom

*e-mail: cenghan515@gmail.com, pl@st-andrews.ac.uk

Supplementary Information

Figure S1. The full-range (left) and expanded (right) PXRD data for (a) (2-BrbaH)$_2$CuCl$_4$, (b) (3-BrbaH)$_2$CuCl$_4$ and (c) (4-BrbaH)$_2$CuCl$_4$.

Figure S2. The full-range (left) and expanded (right) PXRD data for (a) (2-BrbaH)$_2$CuBr$_4$, (b) (3-BrbaH)$_2$CuBr$_4$ and (c) (4-BrbaH)$_2$CuBr$_4$.

Figure S3. Full-range and expanded (inset) Rietveld plot (PXRD) for (a) (2-BrbaH)$_2$CuCl$_4$, (b) (3-BrbaH)$_2$CuCl$_4$ and (c) (4-BrbaH)$_2$CuCl$_4$. Note that there is a significant preferred orientation. In addition, only unit cell and profile parameters were refined, not atomic parameters. The aim here is merely to demonstrate phase purity, which is confirmed by the elemental analysis.

Figure S4. Full-range and expanded (inset) Rietveld plot (PXRD) for (a) (2-BrbaH)$_2$CuBr$_4$, (b) (3-BrbaH)$_2$CuBr$_4$ and (c) (4-BrbaH)$_2$CuBr$_4$.

Figure S5. Thermogravimetric analysis (TGA) data for (a) (2-BrbaH)$_2$CuCl$_4$, (b) (3-BrbaH)$_2$CuCl$_4$, (c) (4-BrbaH)$_2$CuCl$_4$, (d) (2-BrbaH)$_2$CuBr$_4$, (e) (3-BrbaH)$_2$CuBr$_4$ and (f) (4-BrbaH)$_2$CuBr$_4$.

Figure S6. Crystal structures of (a) (2-BrbaH)$_2$CuBr$_4$, (b) (3-BrbaH)$_2$CuBr$_4$ and (c) (4-

BrbaH)$_2$CuBr$_4$ at 298 K viewed along the *b*-axis. The bottom panels are top-view of the crystal structures, perpendicular to the layer direction, emphasizing the similarities and differences between the $[CuBr_4]_\infty$ layers.

Figure S7. SHG responses of (a) (2/3/4-Brba)$_2$CuCl$_4$ and (b) (2/3/4-Brba)$_2$CuBr$_4$ at ambient temperature.

Figure S8. The nature of the distortion within the inorganic octahedra in (a) (4-BrbaH)$_2$CuCl$_4$, and (b) (4-BrbaH)$_2$CuBr$_4$ at 298 K.

Figure S9. Thermal ellipsoids structures for these six compounds at 298 K.

Figure S10. Hydrogen bonding environments of (a) (2-BrbaH)$_2$CuBr$_4$, (b) (3-BrbaH)$_2$CuBr$_4$ and (c) (4-BrbaH)$_2$CuBr$_4$ at 298 K, highlighting the hydrogen bond distance to the apical bromide.

Figure S11. (a) Magnetic susceptibility χ for (2/3/4-BrbaH)$_2$CuCl$_4$ in the low temperature range of 2-15 K. Magnetic susceptibility χ and its inverse $1/\chi$ with Curie-Weiss fit (red line) for (b) (2-BrbaH)$_2$CuCl$_4$, (c) (3-BrbaH)$_2$CuCl$_4$ and (d) (4-BrbaH)$_2$CuCl$_4$ in the range of 100-300 K.

Figure S12. ZFC and FC curves at 100 Oe from 2 to 20 K for (a) (2-BrbaH)$_2$CuCl$_4$, (b) (3-BrbaH)$_2$CuCl$_4$, (c) (4-BrbaH)$_2$CuCl$_4$, from 2 to 26 K for (d) (2-BrbaH)$_2$CuBr$_4$, (e) (3-BrbaH)$_2$CuBr$_4$, (f) (4-BrbaH)$_2$CuBr$_4$.

Figure S13. The ferromagnetic hysteresis loops of (a-c) (2/3/4-BrbaH)$_2$CuCl$_4$ at 2, 5 and 200 K, (d-f) (2/3/4-BrbaH)$_2$CuBr$_4$ at 2, 5 10 and 20 K. Inset: corresponding low-field region of the hysteresis loops.

Figure S14. (a) The correlation between the interoctahedral distortion Cu-Cl-Cu and T_C, (b) R_L and T_C for A_2CuCl_4 structures.

Figure S15. (a) The correlation between R_L and T_C, (b) octahedral distortion and T_C, (c) interoctahedral distortion Cu-Br-Cu and T_C for (2/3/4-BrbaH)$_2$CuBr$_4$ structures.

Table S1. Crystal and Refinement Data for (2-BrbaH)$_2$CuX$_4$ (X = Cl or Br), (3-BrbaH)$_2$CuBr$_4$ and (4-BrbaH)$_2$CuCl$_4$ at 173 K.

Table S2. Hydrogen bond lengths (Å) and angles (°) for (2-BrbaH)$_2$CuCl$_4$ at 298 K.

Table S3. Hydrogen bond lengths (Å) and angles (°) for (3-BrbaH)$_2$CuCl$_4$ at 298 K.

Table S4. Hydrogen bond lengths (Å) and angles (°) for (4-BrbaH)$_2$CuCl$_4$ at 298 K.

Table S5. Hydrogen bond lengths (Å) and angles (°) for $(2\text{-BrbaH})_2CuBr_4$ at 298 K.

Table S6. Hydrogen bond lengths (Å) and angles (°) for $(3\text{-BrbaH})_2CuBr_4$ at 298 K.

Table S7. Hydrogen bond lengths (Å) and angles (°) for $(4\text{-BrbaH})_2CuBr_4$ at 298 K.

Figure S16. The Curie-Weiss fit of the χ -T data for $(2\text{-Brba})_2CuBr_4$ compound between 20-300 K.

Table S8. The Weiss constant θ_1 and θ_2 obtained from the fitting of $1/\chi$ -T data and χ -T data, respectively.

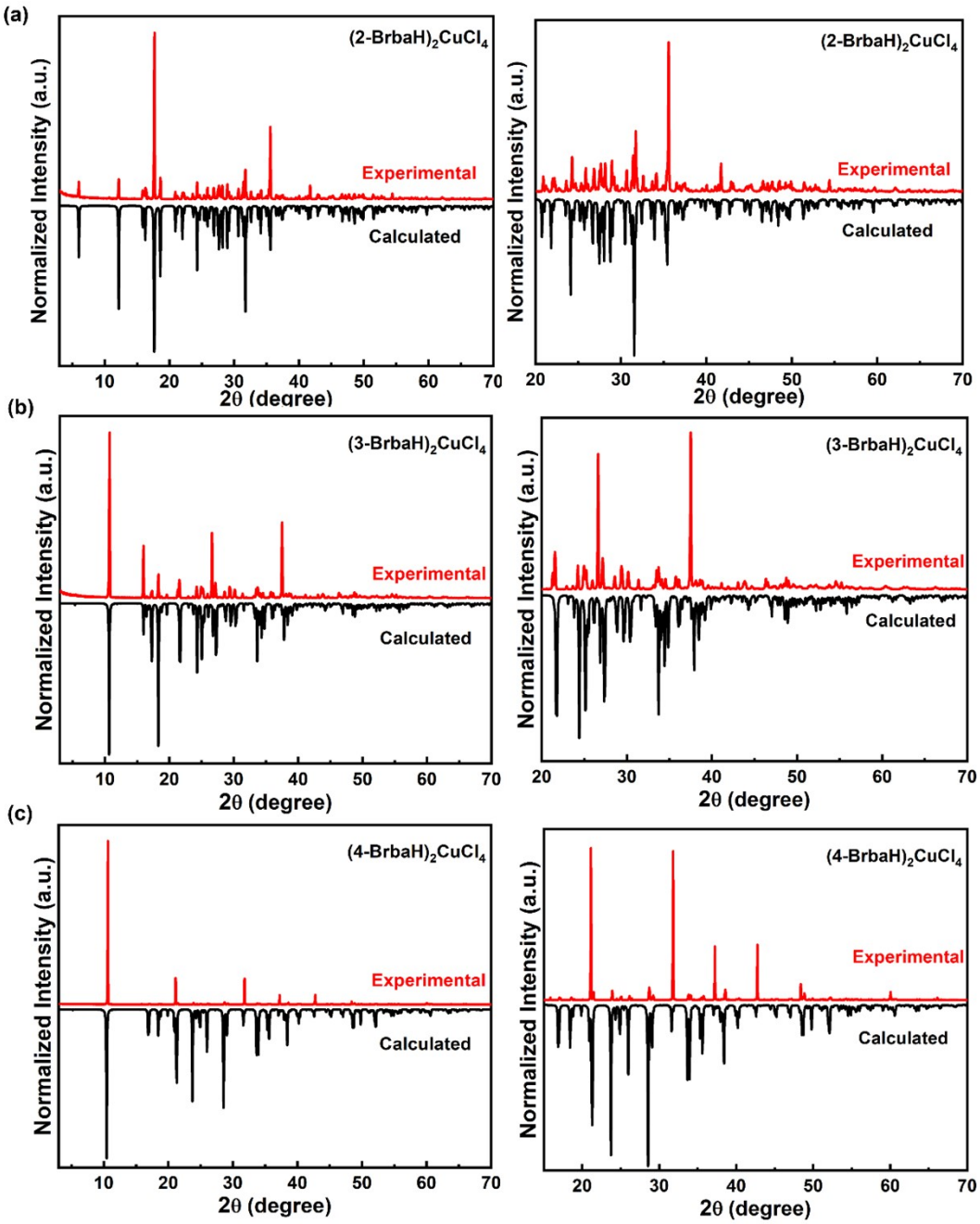

Figure S1. The full-range (left) and expanded (right) PXRD data for (a) (2-

BrbaH)$_2$CuCl$_4$, (b) (3-BrbaH)$_2$CuCl$_4$ and (c) (4-BrbaH)$_2$CuCl$_4$.

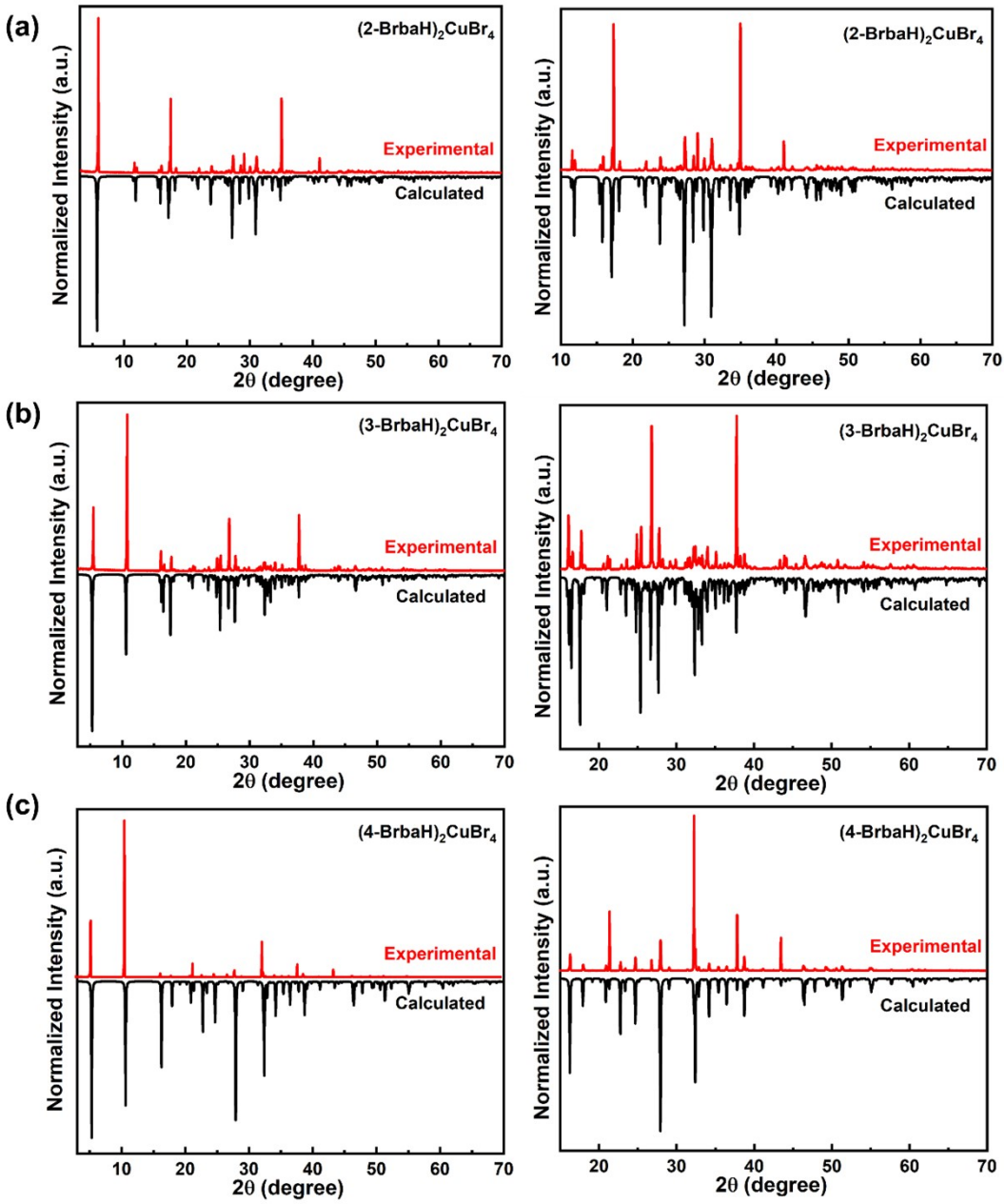

Figure S2. The full-range (left) and expanded (right) PXRD data for (a) (2-BrbaH)$_2$CuBr$_4$, (b) (3-BrbaH)$_2$CuBr$_4$ and (c) (4-BrbaH)$_2$CuBr$_4$.

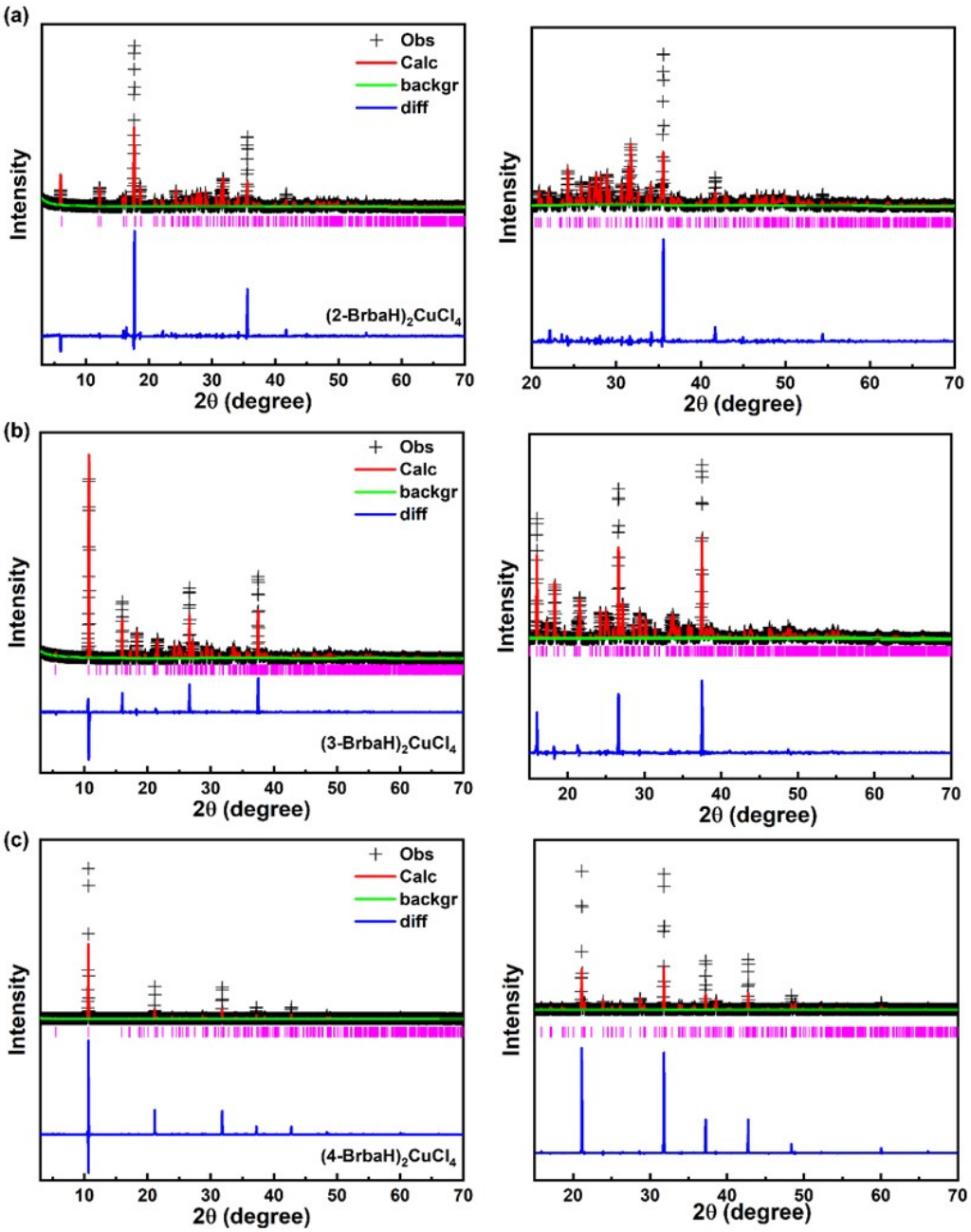

Figure S3. Full-range and expanded (inset) Rietveld plot (PXRD) for (a) (2-BrbaH)$_2$CuCl$_4$, (b) (3-BrbaH)$_2$CuCl$_4$ and (c) (4-BrbaH)$_2$CuCl$_4$. Note that there is a significant preferred orientation. In addition, only unit cell and profile parameters were refined, not atomic parameters. The aim here is merely to demonstrate phase purity, which is confirmed by the elemental analysis.

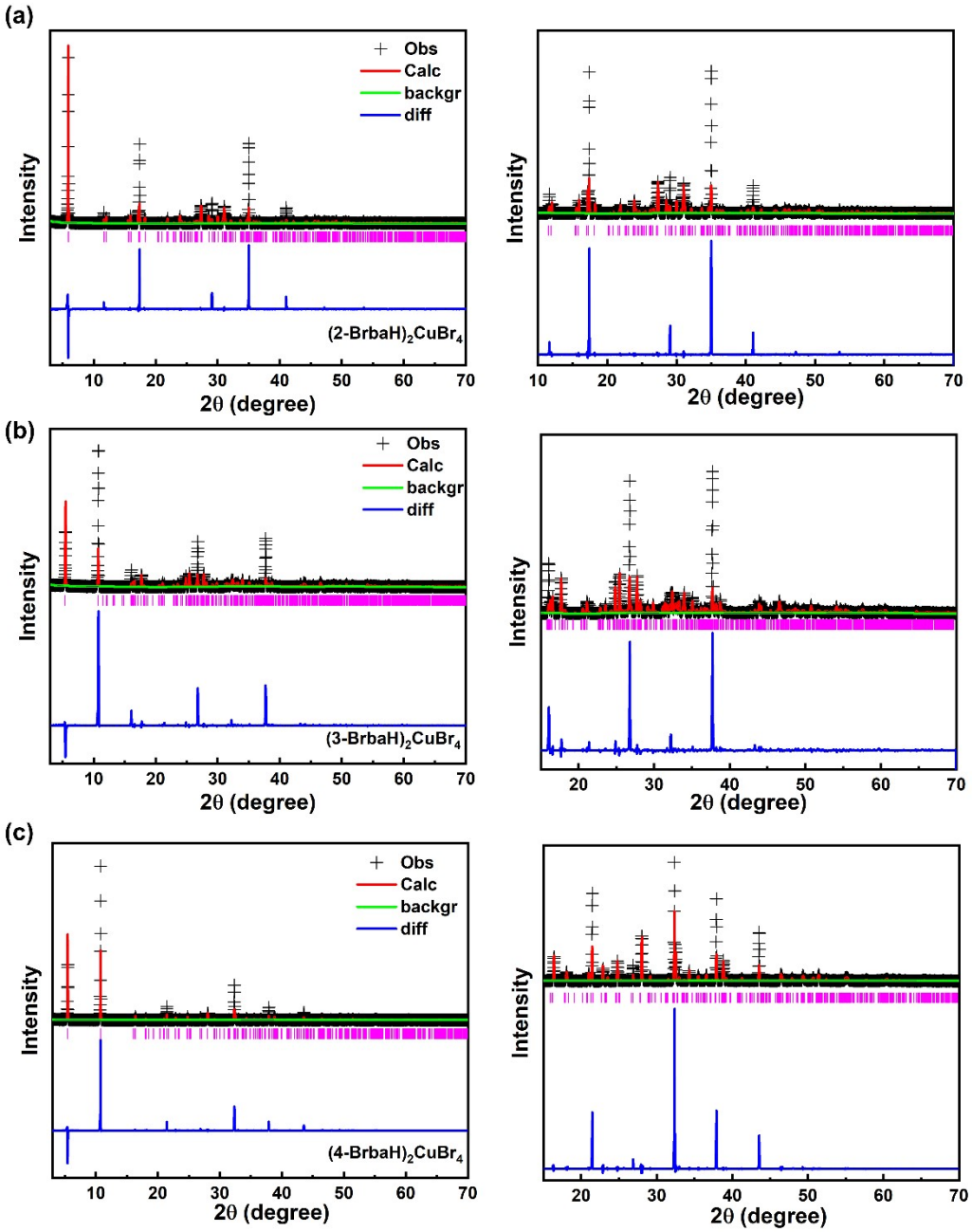

Figure S4. Full-range and expanded (inset) Rietveld plot (PXRD) for (a) (2-BrbaH)$_2$CuBr$_4$, (b) (3-BrbaH)$_2$CuBr$_4$ and (c) (4-BrbaH)$_2$CuBr$_4$.

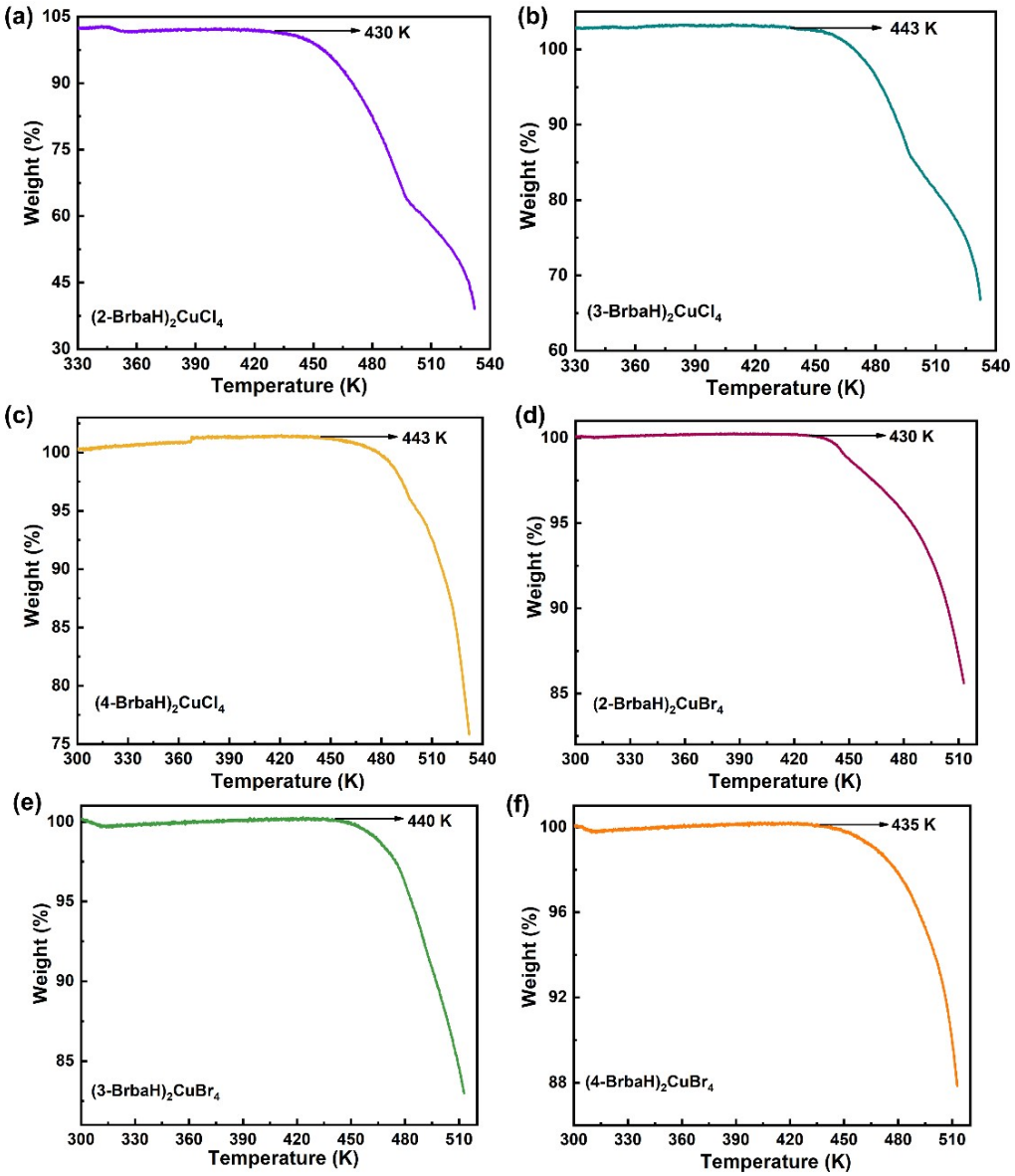

Figure S5. Thermogravimetric analysis (TGA) data for (a) (2-BrbaH)$_2$CuCl$_4$, (b) (3-BrbaH)$_2$CuCl$_4$, (c) (4-BrbaH)$_2$CuCl$_4$, (d) (2-BrbaH)$_2$CuBr$_4$, (e) (3-BrbaH)$_2$CuBr$_4$ and (f) (4-BrbaH)$_2$CuBr$_4$.

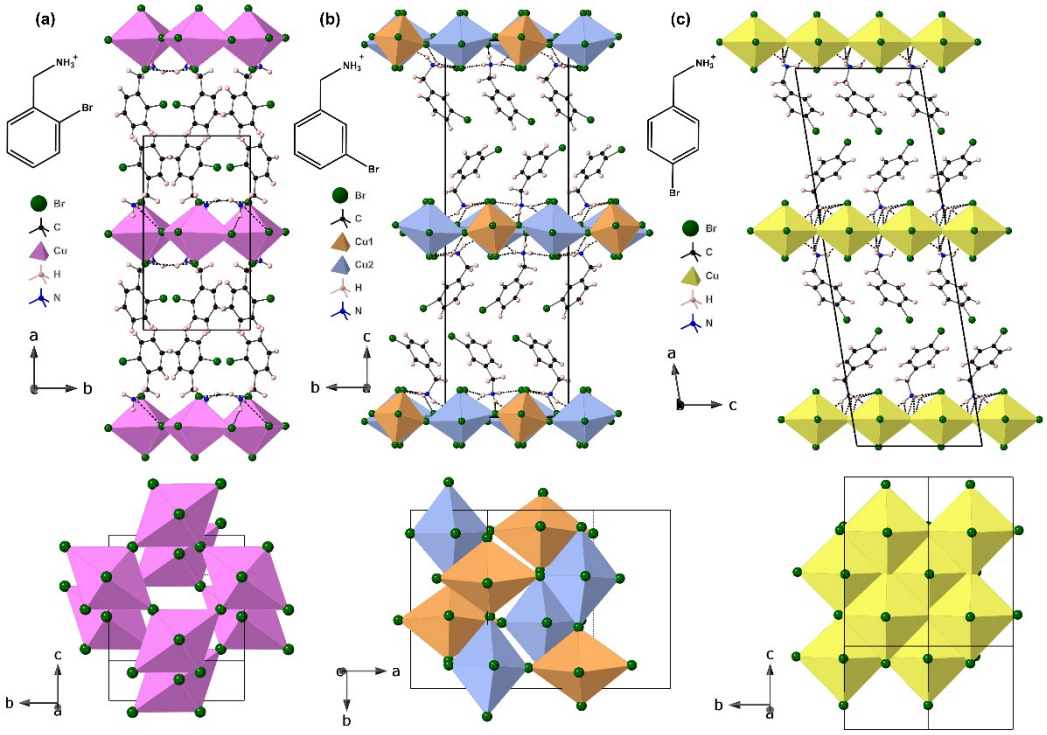

Figure S6. Crystal structures of (a) $(2\text{-BrbaH})_2CuBr_4$, (b) $(3\text{-BrbaH})_2CuBr_4$ and (c) $(4\text{-BrbaH})_2CuBr_4$ at 298 K viewed along the *b*-axis. The bottom panels are top-view of the crystal structures, perpendicular to the layer direction, emphasizing the similarities and differences between the $[CuBr_4]_\infty$ layers.

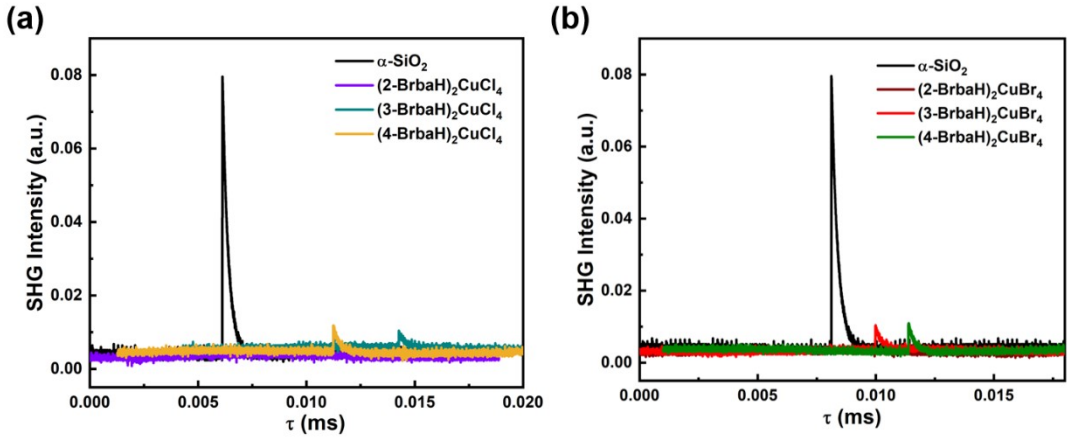

Figure S7. SHG responses of (a) $(2/3/4\text{-Brba})_2CuCl_4$ and (b) $(2/3/4\text{-Brba})_2CuBr_4$ at ambient temperature.

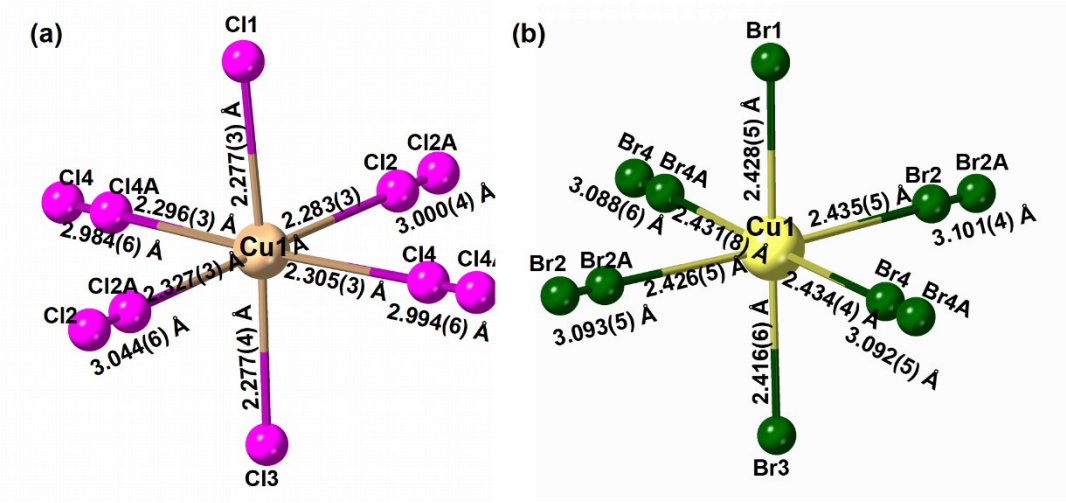

Figure S8. The nature of the distortion within the inorganic octahedra in (a) (4-BrbaH)$_2$CuCl$_4$, and (b) (4-BrbaH)$_2$CuBr$_4$ at 298 K.

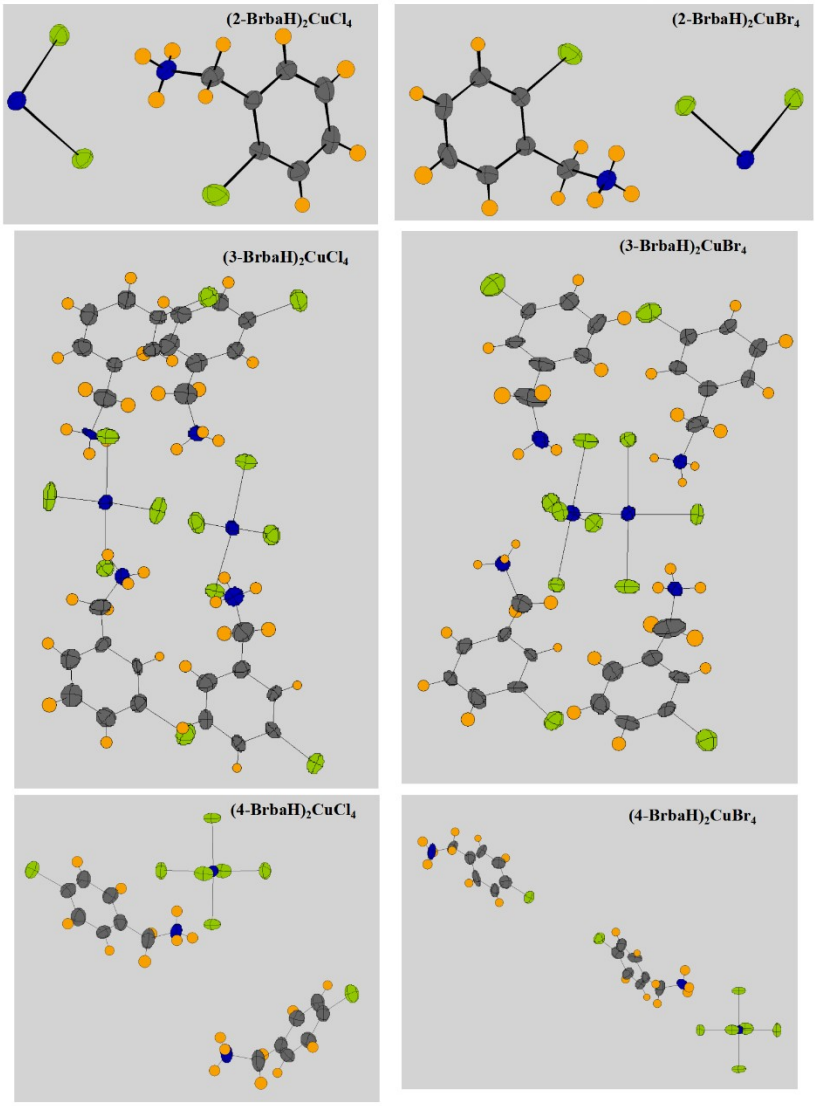

Figure S9. Thermal ellipsoids structures for these six compounds at 298 K.

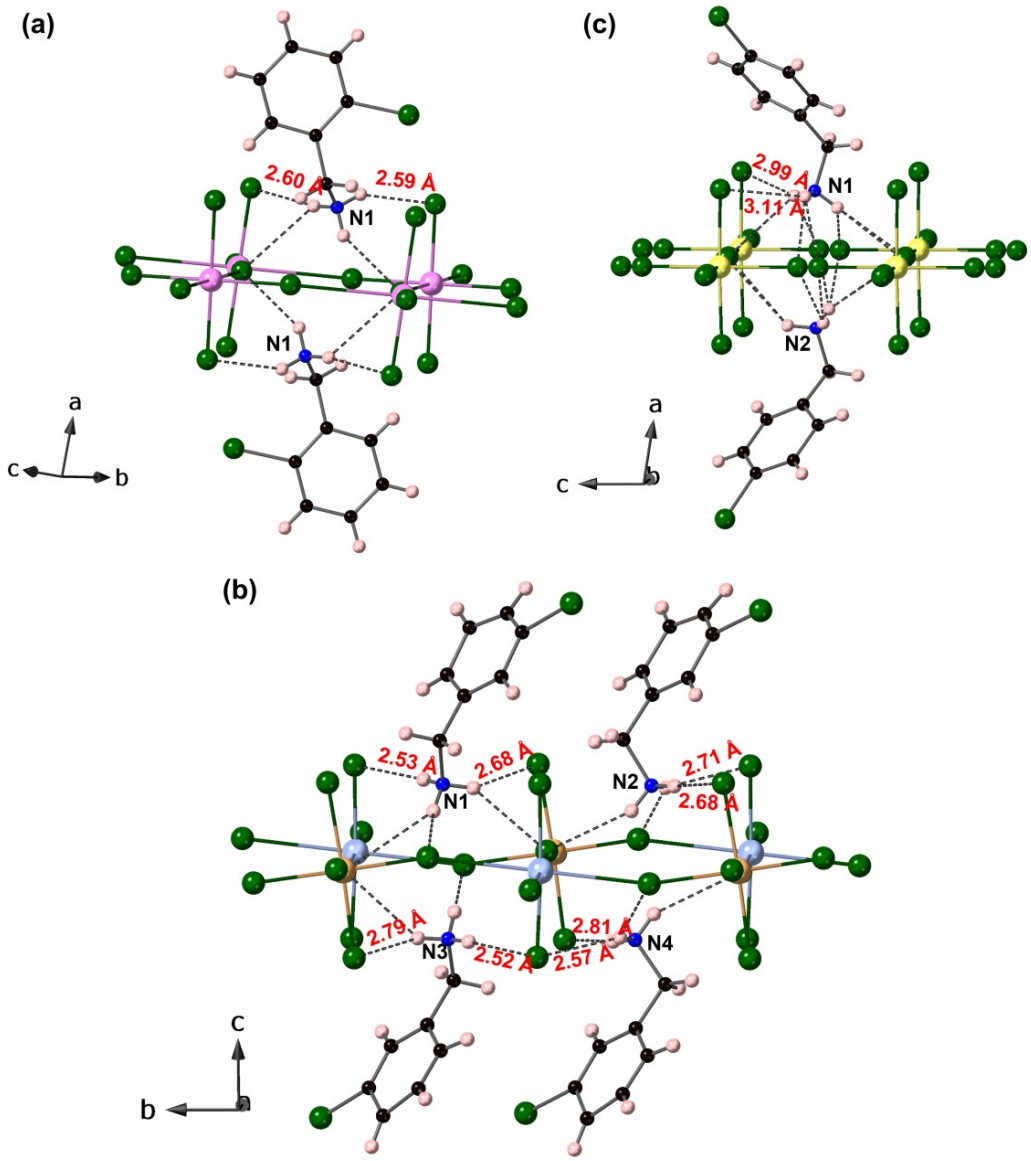

Figure S10. Hydrogen bonding environments of (a) $(2\text{-BrbaH})_2CuBr_4$, (b) $(3\text{-BrbaH})_2CuBr_4$ and (c) $(4\text{-BrbaH})_2CuBr_4$ at 298 K, highlighting the hydrogen bond distance to the apical bromide.

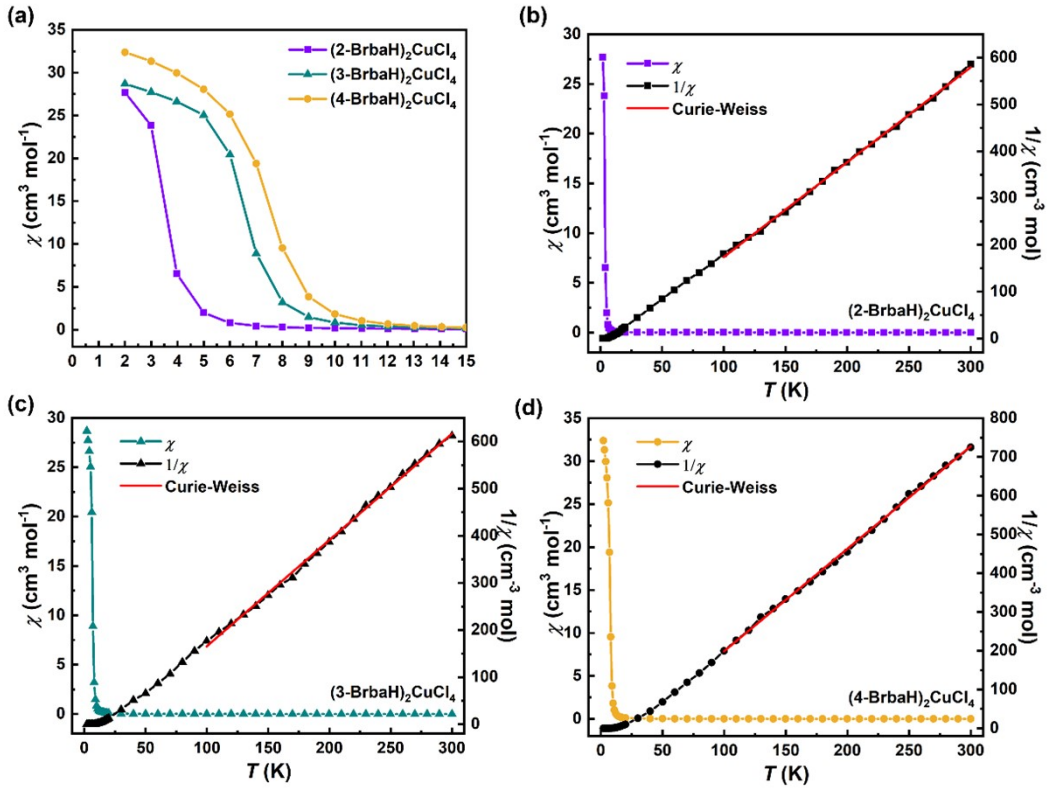

Figure S11. (a) Magnetic susceptibility χ for (2/3/4-BrbaH)$_2$CuCl$_4$ in the low temperature range of 2-15 K. Magnetic susceptibility χ and its inverse $1/\chi$ with Curie-Weiss fit (red line) for (b) (2-BrbaH)$_2$CuCl$_4$, (c) (3-BrbaH)$_2$CuCl$_4$ and (d) (4-BrbaH)$_2$CuCl$_4$ in the range of 100-300 K.

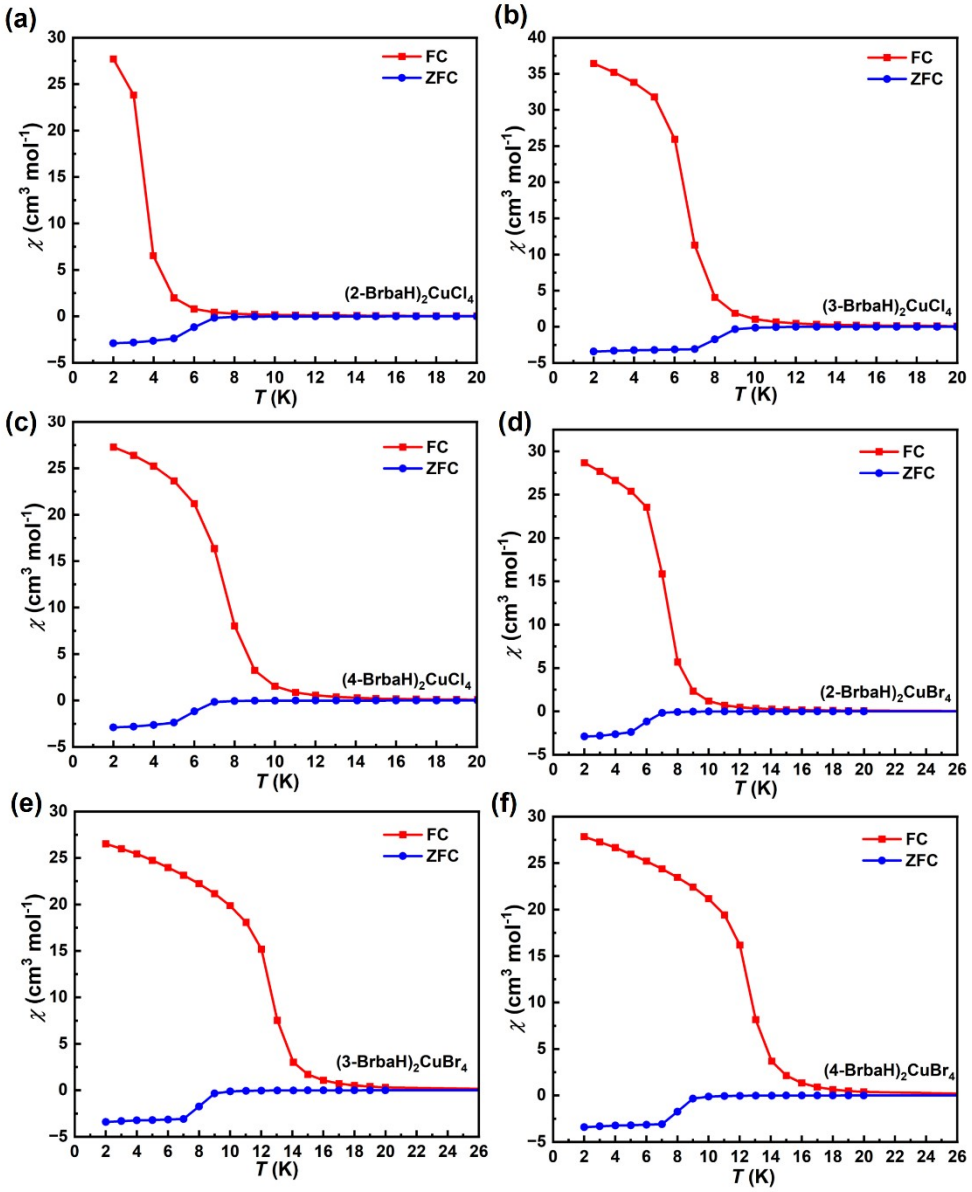

Figure S12. ZFC and FC curves at 100 Oe from 2 to 20 K for (a) $(2\text{-BrbaH})_2CuCl_4$, (b) $(3\text{-BrbaH})_2CuCl_4$, (c) $(4\text{-BrbaH})_2CuCl_4$, from 2 to 26 K for (d) $(2\text{-BrbaH})_2CuBr_4$, (e) $(3\text{-BrbaH})_2CuBr_4$, (f) $(4\text{-BrbaH})_2CuBr_4$.

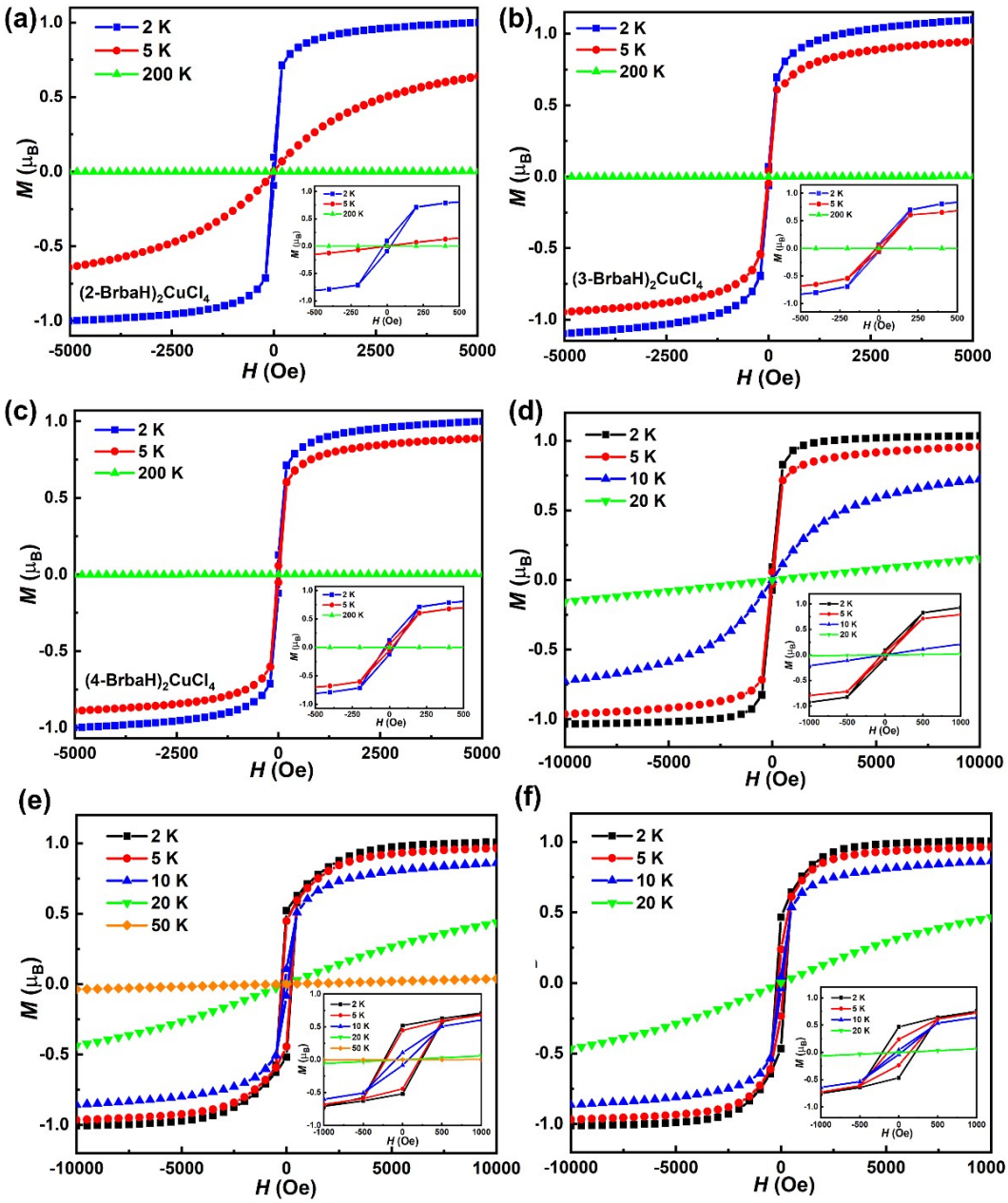

Figure S13. The ferromagnetic hysteresis loops of (a-c) (2/3/4-BrbaH)$_2$CuCl$_4$ at 2, 5 and 200 K, (d-f) (2/3/4-BrbaH)$_2$CuBr$_4$ at 2, 5 10 and 20 K. Inset: corresponding low-field region of the hysteresis loops.

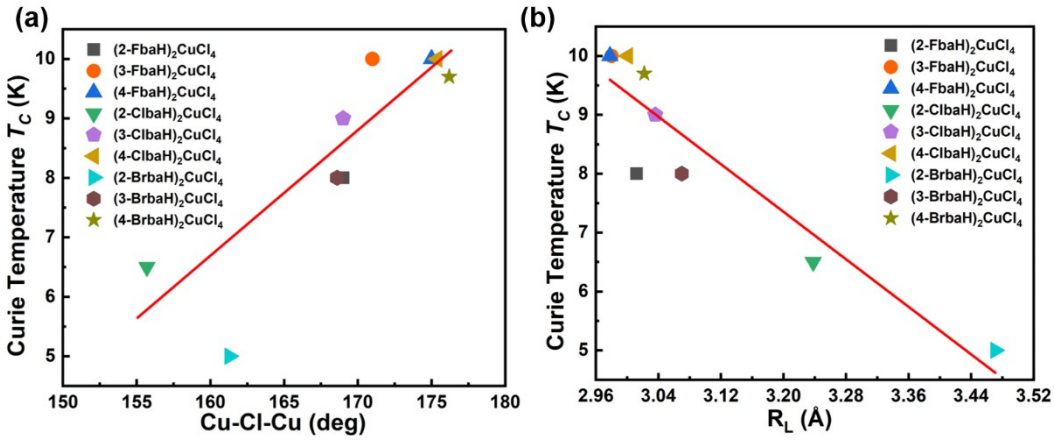

Figure S14. (a) The correlation between the interoctahedral distortion Cu-Cl-Cu and T_C, (b) R_L and T_C for A_2CuCl_4 structures.

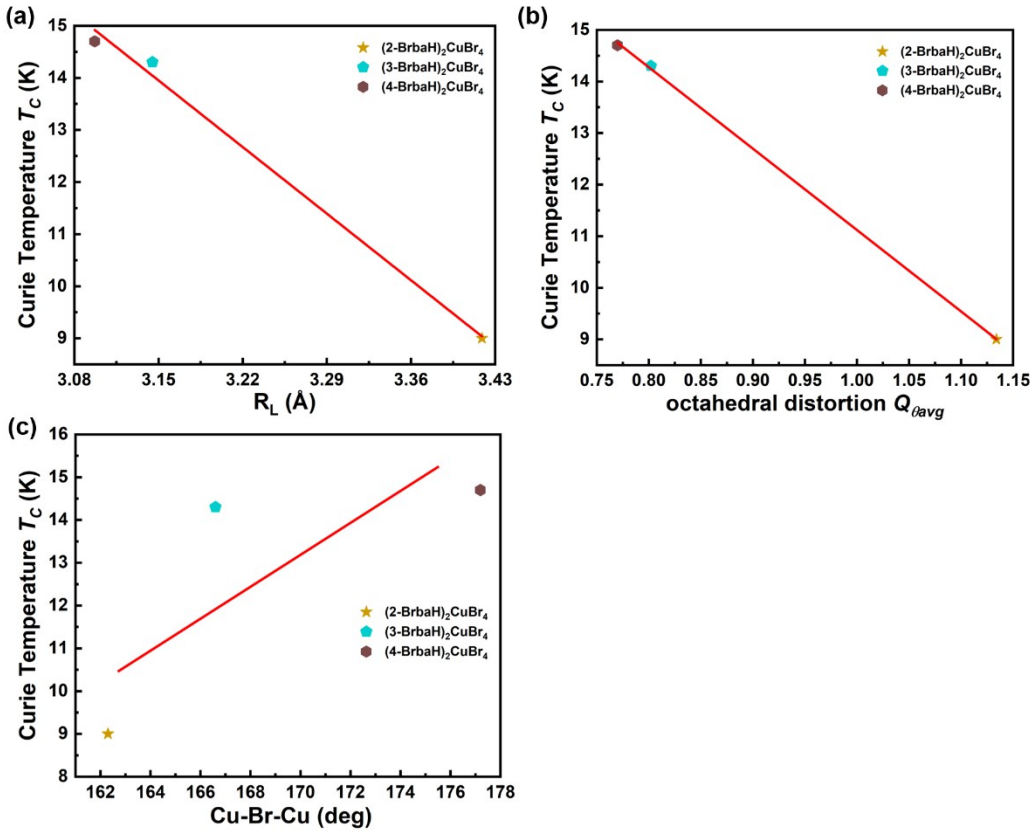

Figure S15. (a) The correlation between R_L and T_C, (b) octahedral distortion and T_C, (c) interoctahedral distortion Cu-Br-Cu and T_C for (2/3/4-BrbaH)$_2$CuBr$_4$ structures.

Table S1. Crystal and Refinement Data for $(2\text{-BrbaH})_2CuX_4$ (X = Cl or Br), $(3\text{-BrbaH})_2CuBr_4$ and $(4\text{-BrbaH})_2CuCl_4$ at 173 K.

compound	**$(2\text{-BrbaH})_2CuCl_4$**	**$(4\text{-BrbaH})_2CuCl_4$**	**$(2\text{-BrbaH})_2CuBr_4$**	**$(3\text{-BrbaH})_2CuBr_4$**
formula	$C_{14}H_{18}N_2Br_2CuCl_4$		$C_{14}H_{18}N_2CuBr_6$	
formula weight	579.46	579.46	757.3	757.3
colour/habit	Green/Platelet	Yellow/Platelet	Purple/Platelet	Purple/Platelet
crystal size (mm^3)	0.40 × 0.40 × 0.20	0.16 × 0.15 × 0.06	0.15 × 0.09 × 0.04	0.21 × 0.19 × 0.02
crystal system	Monoclinic	Monoclinic	Monoclinic	Monoclinic
space group	$P2_1/c$	Cc	$P2_1/c$	Cc
***a* (Å)**	15.3422(11)	34.152(3)	15.5648(10)	11.1694(3)
***b* (Å)**	8.4252(5)	5.2706(4)	8.4891(5)	10.9036(4)
***c* (Å)**	7.6254(5)	10.5890(8)	7.8511(5)	33.6896(13)
α (deg)	90	90	90	90
β (deg)	99.485(4)	98.917(6)	99.206(6)	98.024(3)
γ (deg)	90	90	90	90
***V* ($Å^3$)**	972.19(11)	1883.0(3)	1024.53(11)	4062.8(2)
ρ_{calc} (mg/m^3)	1.979	2.044	2.455	2.476
μ (mm^{-1})	5.781	5.970	12.765	12.876
F(000)	566	1132	710	2840
No. of reflns collected	7539	7212	10140	24675
independent reflns	1641 [R(int) = 0.0307]	3242 [R(int) = 0.0643]	2323 [R(int) = 0.0566]	12480 [R(int) = 0.0516]
goodness of fit	1.059	1.136	0.931	1.048
final *R* indices (*I*	R_1 = 0.0191	R_1 = 0.0481	R_1 = 0.0259	R_1 = 0.0623

> 2σ(*I*))	wR_2 = 0.0476	wR_2 = 0.1353	wR_2 = 0.0579	wR_2 = 0.1397
largest diff. peak/hole (e Å^{-3})	0.705/-0.590	1.049/-0.773	0.674/-0.978	2.747/-1.374

Table S2. Hydrogen bond lengths (Å) and angles (°) for $(2\text{-BrbaH})_2CuCl_4$ at 298 K.

D-H…A	d(D-H)	d(H…A)	d(D…A)	∠(DHA)
N(1)-H(1A)...Cl(1)	0.89	2.46	3.246(3)	146.9
N(1)-H(1B)...Cl(2)#2	0.89	2.53	3.281(3)	142.6
N(1)-H(1C)...Cl(1)#3	0.89	2.43	3.312(3)	172.1
N(1)-H(1C)...Cl(2)#3	0.89	2.88	3.337(3)	113.8

Symmetry transformations used to generate equivalent atoms:

#2 -x+1, y+1/2, -z+1/2; #3 x, -y+1/2, z+1/2

Table S3. Hydrogen bond lengths (Å) and angles (°) for $(3\text{-BrbaH})_2CuCl_4$ at 298 K.

D-H…A	d(D-H)	d(H…A)	d(D…A)	∠(DHA)
N(1)-H(1A)...Cl(2)#1	0.89	2.79	3.45(2)	132.6
N(1)-H(1A)...Cl(8)	0.89	2.82	3.56(2)	142.1
N(1)-H(1B)...Cl(1)	0.89	2.43	3.27(2)	156.4
N(1)-H(1C)...Cl(5)#2	0.89	2.74	3.47(2)	139.8
N(1)-H(1C)...Cl(6)#2	0.89	2.66	3.416(19)	142.9
N(2)-H(2A)...Cl(5)	0.89	2.38	3.26(2)	173.0
N(2)-H(2B)...Cl(4)#3	0.89	2.95	3.49(2)	121.0
N(2)-H(2B)...Cl(6)#4	0.89	2.66	3.46(2)	149.3
N(2)-H(2C)...Cl(1)	0.89	2.66	3.50(2)	157.1
N(2)-H(2C)...Cl(2)	0.89	2.76	3.33(2)	123.3
N(3)-H(3A)...Cl(7)#5	0.89	2.54	3.33(2)	147.8
N(3)-H(3B)...Cl(4)#6	0.89	2.65	3.37(2)	139.0
N(3)-H(3B)...Cl(6)#5	0.89	2.74	3.45(2)	137.1
N(3)-H(3C)...Cl(3)#4	0.89	2.82	3.47(2)	130.5
N(3)-H(3C)...Cl(8)#4	0.89	2.72	3.48(2)	144.5
N(4)-H(4A)...Cl(7)#4	0.89	2.56	3.44(2)	170.1
N(4)-H(4B)...Cl(4)#6	0.89	2.68	3.37(2)	135.2
N(4)-H(4B)...Cl(8)#6	0.89	2.75	3.43(2)	134.0
N(4)-H(4C)...Cl(2)#3	0.89	2.62	3.38(2)	143.2
N(4)-H(4C)...Cl(3)#3	0.89	2.66	3.39(2)	139.8

Symmetry transformations used to generate equivalent atoms:

#1 x+1/2, y-1/2, z; #2 x-1/2, y-1/2, z; #3 x+1/2, y+1/2, z; #4 x-1/2, y+1/2, z; #5 x-1, y+1, z; #6 x, y+1, z

Table S4. Hydrogen bond lengths (Å) and angles (°) for $(4\text{-BrbaH})_2CuCl_4$ at 298 K.

D-H…A	d(D-H)	d(H…A)	d(D…A)	∠(DHA)
N(1)-H(1A)...Cl(3)	0.89	2.92	3.571(10)	130.8
N(1)-H(1A)...Cl(4)	0.89	2.64	3.321(11)	134.0
N(1)-H(1A)...Cl(4A)#2	0.89	2.71	3.365(11)	130.8
N(1)-H(1B)...Cl(2)#5	0.89	2.56	3.409(13)	161.5
N(1)-H(1B)...Cl(2A)#2	0.89	2.59	3.374(13)	148.1
N(1)-H(1B)...Cl(4)#1	0.89	2.88	3.362(11)	115.6
N(1)-H(1B)...Cl(4A)#5	0.89	2.79	3.408(11)	128.1
N(1)-H(1C)...Cl(2)	0.89	2.71	3.338(13)	128.8
N(1)-H(1C)...Cl(2A)#1	0.89	2.63	3.353(13)	139.2
N(1)-H(1C)...Cl(3)#1	0.89	2.82	3.586(11)	144.7
N(2)-H(2A)...Cl(1)#6	0.89	2.87	3.557(10)	134.9
N(2)-H(2A)...Cl(2)#6	0.89	2.77	3.342(13)	123.4
N(2)-H(2A)...Cl(2A)#7	0.89	2.83	3.359(13)	119.3
N(2)-H(2B)...Cl(4)#7	0.89	2.49	3.369(11)	168.5
N(2)-H(2B)...Cl(4A)#8	0.89	2.52	3.406(11)	174.9
N(2)-H(2C)...Cl(2A)#9	0.88	2.86	3.381(13)	119.0
N(2)-H(2C)...Cl(4)#6	0.88	2.61	3.307(12)	136.5
N(2)-H(2C)...Cl(4A)#9	0.88	2.54	3.343(12)	151.4

Symmetry transformations used to generate equivalent atoms:

#1 x, y-1, z; #2 x, -y+1, z+1/2; #3 x, y+1, z; #4 x, -y+1, z-1/2; #5 x, -y, z+1/2; #6 x, y-1, z-1; #7 x, y-2, z-1; #8 x, -y-1, z-1/2; #9 x, -y, z-1/2

Table S5. Hydrogen bond lengths (Å) and angles (°) for $(2\text{-BrbaH})_2CuBr_4$ at 298 K.

D-H…A	d(D-H)	d(H…A)	d(D…A)	∠(DHA)
N(1)-H(1A)...Br(1)#2	0.89	2.59	3.466(3)	170.0
N(1)-H(1A)...Br(2)#3	0.89	2.98	3.444(3)	114.3
N(1)-H(1B)...Br(2)#4	0.89	2.66	3.431(3)	146.2
N(1)-H(1C)...Br(1)	0.89	2.60	3.382(3)	147.8

Symmetry transformations used to generate equivalent atoms:

#1 -x+1, -y+2, -z+1; #2 x, -y+3/2, z+1/2; #3 -x+1, y-1/2, -z+3/2; #4 x, -y+3/2, z-1/2

Table S6. Hydrogen bond lengths (Å) and angles (°) for $(3\text{-BrbaH})_2CuBr_4$ at 298 K.

D-H…A	d(D-H)	d(H…A)	d(D…A)	∠(DHA)
N(1)-H(1A)...Br(1)	0.89	3.13	3.66(2)	120.8
N(1)-H(1A)...Br(8)	0.89	2.53	3.39(3)	163.1
N(1)-H(1B)...Br(6)	0.89	2.68	3.47(3)	148.7
N(1)-H(1B)...Br(7)#1	0.89	3.12	3.54(2)	111.1
N(1)-H(1C)...Br(3)#2	0.89	3.00	3.43(3)	111.6
N(1)-H(1C)...Br(5)#2	0.89	2.77	3.65(3)	172.5
N(2)-H(2A)...Br(6)#2	0.89	2.99	3.45(3)	114.4
N(2)-H(2A)...Br(8)#3	0.89	2.71	3.54(4)	155.6
N(2)-H(2B)...Br(7)#1	0.89	2.68	3.53(4)	161.8
N(2)-H(2C)...Br(1)#3	0.89	3.03	3.46(4)	111.8
N(2)-H(2C)...Br(3)#3	0.89	3.07	3.65(4)	124.7
N(2)-H(2C)...Br(5)#3	0.89	2.60	3.40(3)	150.1
N(3)-H(3A)...Br(4)	0.89	2.52	3.39(3)	165.2
N(3)-H(3B)...Br(1)#1	0.89	2.82	3.57(3)	142.9
N(3)-H(3B)...Br(6)	0.89	3.04	3.65(3)	127.1
N(3)-H(3C)...Br(2)#4	0.89	2.79	3.55(2)	143.5
N(3)-H(3C)...Br(3)#1	0.89	2.88	3.51(3)	129.2
N(4)-H(4A)...Br(1)#5	0.89	2.96	3.51(3)	121.0
N(4)-H(4A)...Br(4)#5	0.89	2.81	3.63(3)	152.6
N(4)-H(4B)...Br(3)	0.89	2.62	3.47(3)	160.8
N(4)-H(4C)...Br(2)#4	0.89	2.57	3.41(3)	157.6

Symmetry transformations used to generate equivalent atoms:

#1 x+1/2, y-1/2, z; #2 x+1/2, y+1/2, z; #3 x+1, y, z; #4 x, y-1, z; #5 x-1/2, y-1/2, z

Table S7. Hydrogen bond lengths (Å) and angles (°) for $(4\text{-BrbaH})_2CuBr_4$ at 298 K.

D-H…A	d(D-H)	d(H…A)	d(D…A)	∠(DHA)
N(1)-H(1A)...Br(2)#1	0.89	2.98	3.48(2)	116.8
N(1)-H(1A)...Br(3)#1	0.89	2.80	3.48(3)	134.4
N(1)-H(1A)...Br(3A)#5	0.89	2.91	3.47(3)	122.7
N(1)-H(1A)...Br(4)#1	0.89	2.99	3.81(2)	152.9
N(1)-H(1B)...Br(2A)#6	0.89	3.01	3.50(2)	116.3
N(1)-H(1B)...Br(3)#7	0.89	2.64	3.48(3)	157.1
N(1)-H(1B)...Br(3A)#6	0.89	2.61	3.49(3)	171.4
N(1)-H(1C)...Br(2)#5	0.89	2.78	3.49(2)	138.0

N(1)-H(1C)...Br(2A)#7	0.89	2.85	3.51(2)	131.8
N(1)-H(1C)...Br(4)#5	0.89	3.11	3.84(2)	140.3
N(2)-H(2A)...Br(3)#8	0.89	2.84	3.53(3)	136.2
N(2)-H(2A)...Br(3A)#9	0.89	2.84	3.54(3)	136.4
N(2)-H(2B)...Br(2)#8	0.89	2.74	3.52(2)	145.8
N(2)-H(2B)...Br(2A)#10	0.89	2.68	3.53(2)	159.6
N(2)-H(2B)...Br(3)#11	0.89	3.07	3.53(3)	114.4
N(2)-H(2B)...Br(3A)#10	0.89	2.95	3.55(3)	126.3
N(2)-H(2C)...Br(2)#9	0.89	2.82	3.52(2)	137.0
N(2)-H(2C)...Br(2A)#11	0.89	2.76	3.54(2)	146.6

Symmetry transformations used to generate equivalent atoms:

#1 x, -y, z-1/2; #2 x, y-1, z; #3 x, -y, z+1/2; #4 x, y+1, z; #5 x, -y+1, z-1/2; #6 x, y, z-1; #7 x, y+1, z-1; #8 x+1/2, y+5/2, z-2; #9 x+1/2, y+3/2, z-2; #10 x+1/2, -y+5/2, z-5/2; #11 x+1/2, -y+3/2, z-5/2

We tried to fit the χ-T data at higher temperature. This type fitting yields similar Weiss constants to the fitting of $1/\chi$-T data, as shown in the below Table S8. An example of $(2\text{-Brba})_2CuBr_4$ compound is shown in Figure S16, which is fitted between 20-300 K. For the Cu-based perovskites, researchers usually fit the $1/\chi$-T data to obtain the Curie constant C and Weiss constant θ.[1,2] On the other hand, here we focus on the positivity or negativity of the Weiss constant. The positive Weiss temperature is further evidence supporting the existence of ferromagnetic interactions.

1. B. Sun, Z. Yan, Y. Cao, S. Ding, R. Li, B. Ma, X. Y. Li, H. Yang, W. Yin, Y. Zhang, Q. Wang, X. Shao, D. Yang, D. Xue, H. L. Zhang, *Adv. Mater.*, 2023, **35**, 2303945.

2. Y. P. Gong, X. X. Chen, G. Z. Huang, W. X. Zhang, X. M. Chen, *J. Mater. Chem. C.*, 2022, **10**, 5482-5488.

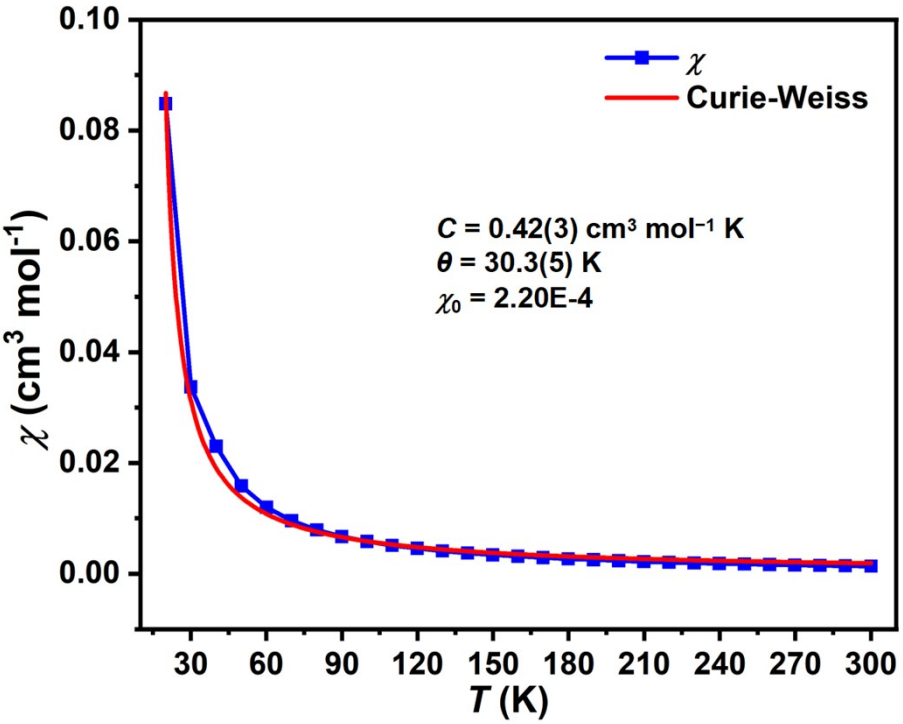

Figure S16. The Curie-Weiss fit of the χ -T data for (2-Brba)$_2$CuBr$_4$ compound between 20-300 K.

Table S8. The Weiss constant θ_1 and θ_2 obtained from the fitting of $1/\chi$ -T data and χ -T data, respectively.

Compound	θ_1 (K)	θ_2 (K)
(2-BrbaH)$_2$CuCl$_4$	24.6(3)	20.2(2)
(3-BrbaH)$_2$CuCl$_4$	31.4(2)	28.3(3)
(4-BrbaH)$_2$CuCl$_4$	33.6(4)	29.5(3)
(2-BrbaH)$_2$CuBr$_4$	36.8(5)	30.3(5)
(3-BrbaH)$_2$CuBr$_4$	59.4(3)	52.7(4)
(4-BrbaH)$_2$CuBr$_4$	65.2(2)	58.3(2)